SAND2008-1964C

<SC-11>

Liquid-Phase Diesel Spray Penetration during End-of-Injection Transient

*Sanghoon Kook[1], Lyle M. Pickett[1], Mark P. B. Musculus[1], and Ryan K. Gehmlich[2]

[1]*Sandia National Laboratories, 7011 East Ave., Livermore, CA94551, USA*
[2]*University of California, Davis, One Shields Avenue, Davis, CA95616, USA*

Key Words: Diesel Spray, End of Injection, Shadowgraph, Mie-Scatter, Entrainment Model

ABSTRACT

Many strategies for low-emissions diesel combustion operate with a positive ignition dwell mode, where the ignition delay exceeds the injection duration. Although nitrogen oxides and particulate matter emissions can be reduced, unburned hydrocarbon and carbon monoxide emissions typically increase. Sources of these emissions can stem from characteristics of the fuel spray after the end of injection, which may differ significantly from the main injection period where most spray models have been developed. To provide fundamental details of spray mixing during the end-of –injection transient, we have studied liquid-phase penetration and evaporation using simultaneous high-speed shadowgraph and Mie-scatter imaging for a single-hole, common-rail injector. Experiments were conducted over a wide range of ambient temperature and density in a constant-volume vessel.

The experiments show that the maximum liquid penetration distance decreases (recedes towards the injector) from the quasi-steady-state distance during the injection-rate ramp-down for most diesel conditions. A transient jet entrainment model, coupled with the assumption of mixing-limited spray vaporization and direct measurement of the vaporized jet spreading angle, shows that this behavior is caused by a slower fuel delivery interacting with an increased rate of ambient entrainment during the injection-rate ramp-down. This increased mixing travels downstream as an "entrainment wave," permitting complete vaporization at distances closer to the injector than the quasi-steady liquid length. The position of the entrainment wave relative to the quasi-steady liquid length determines how far, and how quickly, liquid recedes towards the injector. The tendency of recession increases with increasing ambient temperature and density because the entrainment wave interacts with a liquid region that is originally closer to the nozzle. Alternatively, the liquid length recession is zero for conditions with low ambient temperature or density because the quasi-steady liquid length is downstream of the entrainment wave.

INTRODUCTION

Prior to the start of combustion, diesel fuel injection includes mixing processes such as the breakup of liquid fuel (atomization)[1], hot charge-gas entrainment [2-3], fuel vaporization [4], and molecular-scale mixing of vaporized fuel. The fuel-ambient mixing process is significant because it affects the entire diesel spray combustion and emissions formation event.

Diesel spray penetration and mixing have been studied extensively [5-9] and simplified models exist to describe the tip penetration, overall ambient entrainment, and liquid vaporization [10]. The extent of liquid-phase penetration within the developing fuel jet is strongly affected by ambient and injector conditions. The liquid-phase spray reaches a maximum penetration length that is nearly constant during the steady period of injection, while the vapor-phase of the spray continues to penetrate downstream [4, 7-9]. Presenting data over a wide range of ambient and injector conditions, Siebers [11] shows that this liquid length is ultimately limited by mixing. Sufficient ambient thermal energy and mass are mixed into the spray to produce local thermodynamic conditions where the fuel is vapor phase. This understanding has led to the improvement of diesel spray models for injections with quasi-steady liquid penetration.

Although traditional diesel combustion involves timings where injection and combustion overlap and are quasi-steady, modern low-temperature combustion modes of operation typically involve combustion with positive ignition dwell; that is, the ignition delay exceeds the injection duration. As such, the liquid mixing and vaporization are dominated by events occurring *after* the end of injection (EOI). The fuel-ambient mixtures that result are generally more fuel lean (equivalence ratio < 1), thereby benefitting engine-out nitrogen oxides and particulate matter emissions. However, unburned hydrocarbon (UHC) emissions typically increase [12-14]. Recent studies show that a fuel-lean mixture is formed in the upstream (near nozzle) region of the fuel spray shortly after EOI [15-16]. This near-nozzle mixture fails to burn to completion and becomes a source of UHC emissions [16]. A detailed understanding of the spray vaporization and mixing processes after EOI is needed to

understand the production of fuel-lean mixtures near the injector, and to prevent these mixtures from becoming UHC emissions.

Shortly before EOI, the fuel injection velocity and mass flow rate decline while the injector needle valve closes. Knowledge about how this injection ramp-down affects fuel-ambient mixing is limited. Aside from the observation that the near-nozzle mixture quickly becomes fuel-lean after the liquid evaporates, studies have noted that the ambient gas entrainment does not decrease [15] and that the mixture becomes stagnant (has low-momentum) after EOI [16] . Currently, however, the behavior of the liquid-phase portion of the spray, and its interaction with the downstream fuel jet, is not well understood.

The objective of this study is to provide fundamental information about the liquid-phase spray penetration and evaporation after EOI. Simultaneous liquid- and vapor-phase spray imaging was performed using high-speed imaging systems. The ambient gas temperature and density were varied while using the same common-rail injector (constant injection ramp-down) to determine how charge-gas parameters affect liquid-phase penetration after EOI. In addition, a one-dimensional jet entrainment model based on a discrete control-volume analysis was used to aid interpretation of the experimental results.

EXPERIMENTAL SETUP

The end-of-injection spray was studied in an optically accessible, constant-volume vessel under simulated, quiescent diesel engine conditions. A schematic of the vessel along with the optical setup is shown in Fig. 1. More details about the vessel geometry, fuel injection system, and ambient condition generation are found in [17]. Here, we provide a brief summary.

The vessel has a cubical chamber, 108 mm on each side. Sapphire windows are located in three side ports of the chamber to allow line-of-sight and orthogonal imaging of the injected fuel spray. A Bosch common-rail injector with a single-hole, mini-sac nozzle is mounted in a metal side-port, directing a spray into the center of the chamber. The rate of injection was determined by a momentum measurement and total injected mass measurement at the same fuel temperature, injection duration, and injection pressure as in the imaging experiment. The rate-of-injection technique was similar that described in [11].

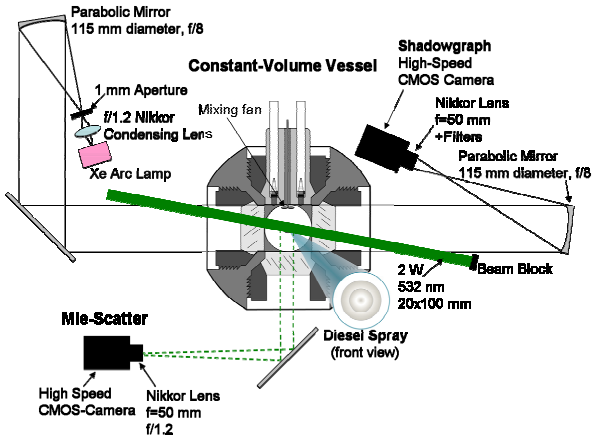

Fig. 1 Constant-volume vessel. Also shown are shadowgraph and Mie-Scatter optical setup.

Experiments were performed at the specified ambient gas temperature and density in an environment with 0% oxygen. This non-reacting condition was selected intentionally to isolate the mixing and vaporization processes from more complex effects of combustion. The studied temperature and density conditions are listed in Table 1.

Two high-speed images were collected simultaneously as shown in Fig. 1. One was a Mie-scatter image to analyze liquid-phase spray penetration. A continuous-wave Nd:YAG laser (532 nm) operating with 2 W power was used for the light source. The laser beam was formed into a 100-mm wide and 20-mm thick sheet to illuminate the spray. A high-speed CMOS camera (IDT X-Vision) fitted with a 532-nm bandpass filter (10 nm FWHM) and a 50-mm focal length, f/1.2 lens collected Mie-scattered light from fuel droplet at 50,000 frames per second. The lens aperture (f/1.2) and camera exposure time (17 μs) were selected to intentionally saturate pixels in dense regions of the spray, thus providing the sensitivity needed to identify low-intensity regions where liquid completely vaporizes. The other high-speed imaging technique was a shadowgraph system, capable of detecting refractive index gradients at the boundary between vaporized fuel and hotter ambient gases. A 150 W (electrical power) mercury-xenon arc lamp was the white light source. To obtain a high-quality point source, the emitted beam passed through a 50-mm focal length f/1.2 Nikkor lens and 1-mm aperture. The beam was then collimated by an f/8 mirror with a 115-mm diameter, passed through the vessel and then refocused to the other high-speed CMOS camera (Phantom v7.1) equipped with a 50-mm focal length Nikkor lens. Images were collected at 75,471 frames per second, 2-μs exposure duration, and with 256 by 64 pixel resolution. A zero-incidence 532-nm mirror was used to block laser scatter from liquid droplets.

Table 1 Experimental conditions

Injector conditions	
Type	Bosch common-rail
Nozzle	Single-hole, KS1.5/0.86
Nozzle diameter	90 μm
Injection pressure	150 MPa
Ambient conditions	
Oxygen	0 %
Temperature	767 ~ 1150 K
Density	5.2 ~ 31.5 kg/m^3
Fuel conditions	
Type	No. 2 Diesel
Density at 288 K	843 kg/m^3
Temperature	373 K

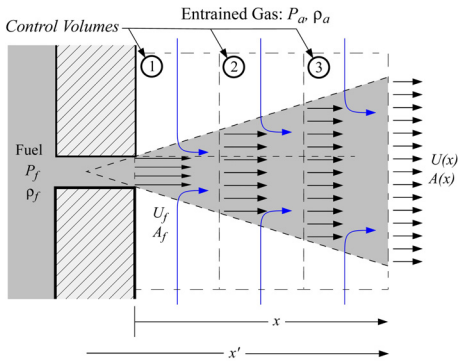

Fig. 2 Discrete control-volume analysis of jet mixing

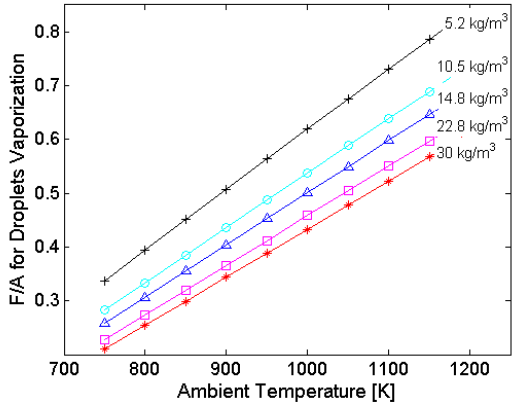

Fig. 3 Fuel-to-ambient ratio for complete liquid vaporization (saturated thermodynamic state of the mixture) over a range of ambient temperatures and densities. Fuel is heptadecane, as a surrogate for No. 2 diesel liquid penetration [11], at an initial temperature of 373 K.

JET MIXING MODEL

A simplified model for jet mixing was exercised to aid interpretation of the experimental results. A schematic of the model is shown in Fig. 2. The jet model consists of a one-dimensional array of discrete control volumes in the axial direction of the jet. Mass and momentum transport between control-volumes is solved numerically. The overall concept for the control-volume model is similar to that offered by Naber and Siebers [10]. They successfully used a *single* control volume and the assumption of a constant jet spreading angle to model experimental jet penetration and fuel-ambient mixing based on a derived analytical solution. However, the Naber and Siebers model applies only to fuel jets with constant injection velocity and therefore cannot be used to describe injection ramp-down. By using many control volumes, variable injection rates are permissible in the discrete jet mixing model of Fig. 2. The discrete control-volume model continues to assume that the spreading angle of the jet is constant, even after the end of injection. Justification for this assumption is supported by our shadowgraph imaging and other measurements as will be discussed below.

In contrast to the Naber and Siebers model (and the schematic of Fig. 2), a polynomial radial profile for mixing and velocity that approximates real jet distribution was also implemented in the new jet model. The velocity and fuel mass distribution are therefore higher in the center of the jet, and more realistic [18]. A more realistic radial profile significantly impacts the momentum and mass transport in the jet, as high-momentum fluid tends to penetrate quickly through the center of the spray in comparison to a uniform velocity over the jet cross-section. Unfortunately, the limited space allotted to this paper does not permit a full description of the numerical techniques used in the control-volume model, but further details will be forthcoming in a future publication.

The control-volume model provides solutions for the fuel-ambient mixture throughout the jet, but makes no distinction between liquid or vaporized fuel (it also assumes no velocity slip between the fuel and ambient). Following Siebers [11], we therefore assume that the fuel vaporization is mixing-limited, meaning that the liquid-phase boundary corresponds to a particular fuel-to-ambient ratio (F/A) where local thermodynamic conditions for this mixture are sufficient to vaporize the liquid. The F/A for liquid vaporization depends upon the fuel and ambient properties at a given experimental condition, as shown in Fig. 3. This particular F/A is highlighted in the model results to indicate the liquid-phase boundary.

RESULTS AND DISCUSSIONS

In this section, we present simultaneous Mie-scatter and shadowgraph imaging results to demonstrate characteristics of the liquid and vapor regions of the spray after EOI. Experimental results for ambient temperature and density variation are then given. Finally, jet mixing model simulations are shown to clarify causes for the observed behavior of the liquid-phase spray.

Figure 4 shows an example of simultaneous liquid and vapor-phase imaging for the temporal development of the spray shortly after start of injection (ASI). The Mie-scattered image at the left shows a bright, saturated region at the dense region of the spray and decreasing intensity at the tip of the spray. To aid in visualization of the liquid-phase boundary, connecting lines are overlaid on the image at 8/256 intensity counts. This liquid boundary is also superimposed on the shadowgraph images, which correspond to the vapor boundary of the spray. Note that the shadowgraph background has a non-uniform small-scale structure in the ambient gas. This non-uniformity is caused by temperature gradients found in the ambient gases and in boundary layers at the windows of the vessel, and is therefore unavoidable [19]. However, the penetrating jet remains visible above this background with a darker, and more uniform, structure.

The liquid and vapor phases of the spray penetrate together initially, but at about 200 μs ASI, the liquid-phase spray reaches a maximum penetration distance, while the vapor phase of the spray continues

downstream. This "quasi-steady" liquid penetration distance was time-averaged during injection and is shown as a dashed line. As mentioned in the Introduction, this maximum liquid penetration length is observed in typical diesel sprays, and depends upon the ambient and fuel injector conditions [4, 7-9].

For the same condition, liquid- and vapor-phase spray images were captured after end of injection (AEI). The shadowgraph images are shown in Fig. 5 with liquid boundaries overlaid on the images. The quasi-steady liquid length again presented as a dashed-line. Shortly after end of injection, droplets near the fuel injector move downstream, or are vaporized, making the spray detach from the injector nozzle. Next, the liquid region shrinks in all directions. The spray "tip" decreases from the quasi-steady liquid length and the spray "tail"

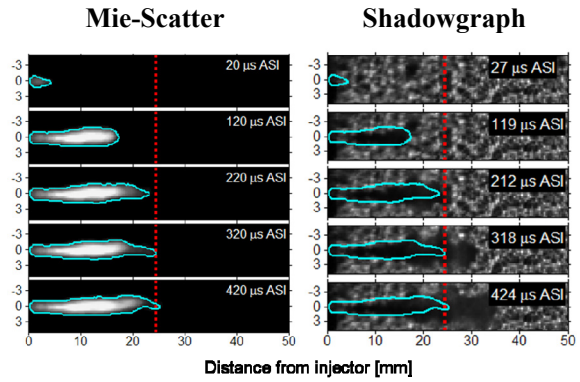

Fig. 4 Simultaneous Mie-Scatter (liquid-phase spray, left) and shadowgraph (vapor-phase spray, right) imaging time sequence after start of injection (ASI). The mean quasi-steady liquid penetration length is shown as a dashed line. Liquid boundaries determined from Mie-Scatter images are overlaid on shadowgraph images. Ambient conditions: 850 K, 14.8 kg/m^3

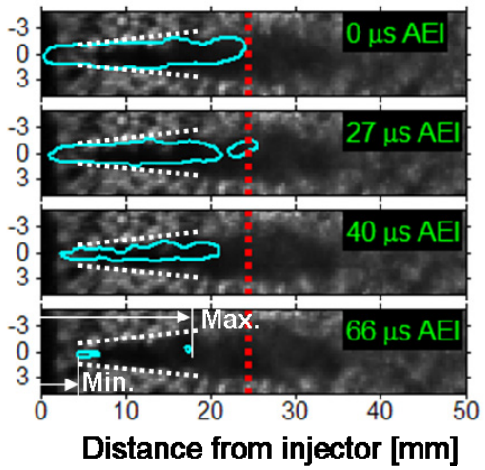

Fig. 5 Shadowgraph (vapor-phase spray) imaging time sequence after end of injection (AEI). Liquid boundaries determined from Mie-scatter images are overlaid on Shadowgraph images. Conditions are the same with Fig. 3.

detaches from the nozzle and continues to penetrate downstream. The liquid border also moves to the center of the spray and complete vaporization occurs by about 70 µs AEI.

From a Lagrangian perspective, if all liquid fuel leaving the injector experienced the same mixing with the ambient, we might have expected that liquid fuel leaving the nozzle after EOI would vaporize at the same quasi-steady liquid length. This hypothesis is further supported by the finding that the quasi-steady liquid length does not depend upon injection pressure [11]; i.e., lower injection velocities produce the same quasi-steady liquid length. The explanation for this behavior is that a slower injection velocity is matched to a slower rate of ambient entrainment, causing mixtures of the same F/A to form at a given axial distance from the injector. However, figure 5 shows that the spray recedes back toward the nozzle from the quasi-steady liquid length, opposite to the general convective direction of the spray. This observation suggests that mixing processes during the EOI transient must somehow be different than ideas developed for quasi-steady fuel sprays.

Measurement of the jet vapor boundary, as well as the injection-rate ramp-down, provide evidence that the fuel-ambient mixing processes are indeed different after EOI. Figure 5 shows relatively dark regions, indicating a fuel vapor boundary, that do not change substantially throughout the EOI transient and liquid-phase vaporization. Although the shadowgraph measurement is somewhat coarse, the immediate conclusion from the images is that the spreading angles of the vapor-phase spray do not decrease after EOI. A lack of significant change in spreading angle is supported by more quantitative measurements of vapor fuel concentration after EOI [16].

The ramp-down in fuel injection rate before EOI, (shown in Fig. 6 to occur over approximately 60 µs) coupled to the finding that the spray spreading angles do not change significantly, implies that the rate of ambient entrainment into the jet increases relative to the rate of fuel delivery. As a result, the F/A would tend to decrease in the near-nozzle region. However, the presence of

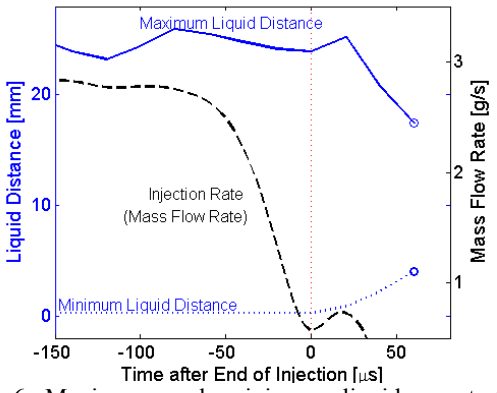

Fig. 6 Maximum and minimum liquid penetration distances along with a fuel mass flow rate before and after end of injection. Ambient conditions: 850 K, 14.8 kg/m^3

liquid and fuel vapor in the near-nozzle region also shows that all of the fuel does not simply convect downstream, leaving only ambient gases in the wake of the spray. The role of this enhanced ambient mixing in the near-nozzle region, and its effect on liquid vaporization for EOI spray, will be discussed throughout the rest of the paper.

Two quantities that can be used to characterize the liquid vaporization after EOI are the maximum (downstream) and minimum (near-nozzle) liquid distances. These distances, which correspond to the liquid boundaries on the images of Fig. 5, are plotted in Fig. 6 together with the injection-rate ramp-down. The figure shows that the minimum liquid distance increases after EOI and maximum liquid distance decreases shortly thereafter. The observed "recession" of the liquid-phase spray penetration distance can also be summarized schematically in Fig. 7. That is, the decline in a maximum liquid distance from the quasi-steady liquid distance is defined as the liquid length recession. The detachment of the liquid spray after EOI results in an increase of the minimum liquid distance.

The effect of ambient temperature on the EOI spray vaporization is presented in Figs. 8 and 9. Five different ambient temperatures were varied while all other operating conditions, including injector hardware, injection pressure, and ambient density held constant. It is notable in Fig. 8 that the ambient temperature has no significant effect on jet spreading angle after EOI. This is consistent with quasi-steady sprays from Ref. [11]. This result suggests that the relative entrainment rate after EOI is not affected by the variations in ambient temperature.

Figure 9 shows that the liquid length recedes when the ambient temperature is greater than 850 K. The time after EOI of liquid recession also tends to decrease with increasing temperature. Open circles indicate the timing when the vaporization process is complete. Note that, for the highest ambient temperatures, some liquid recession even occurs prior to the end of injection, during the injection-rate ramp-down.

On the other hand, the lowest ambient temperature condition, 767 K, experiences no liquid recession from the quasi-steady liquid length. Therefore, an ambient temperature variation shows two different types of liquid vaporization after EOI: those with no liquid length recession at lower ambient temperature, and those with significant liquid length recession at higher ambient temperature.

Similar results were acquired for a variation in ambient density, as shown in Figs. 10-11. In this case, the ambient temperature was held constant at 900 K. Results show that the lowest ambient density condition (5.22 kg/m^3) has no liquid length recession. Rather, the liquid spray divides into several regions, but the largest region, and the last to vaporize, remains near the quasi-steady liquid length prior to complete vaporization. However, for all higher density conditions, the liquid length recedes after EOI.

To examine the causes for the liquid vaporization behavior after EOI, F/A mixing was simulated using the discrete control-volume jet entrainment model and the measured injection-rate ramp-down. Figure 12 shows calculated time sequences of liquid-phase spray boundaries for various ambient temperatures corresponding to Figs. 8-9. Recall that the liquid boundary in the model is assumed to be the F/A ratio for mixing-limited vaporization given in Fig. 3 and it depends upon the ambient temperature, and density.

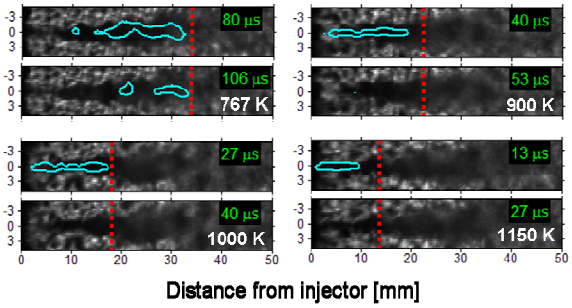

Fig. 8 Liquid-phase spray boundary overlaid on shadowgraph images for various ambient temperatures. Near complete vaporization timings after end of injection (AEI) are shown. Dashed lines are quasi-steady liquid lengths. Ambient density is 14.8 kg/m^3.

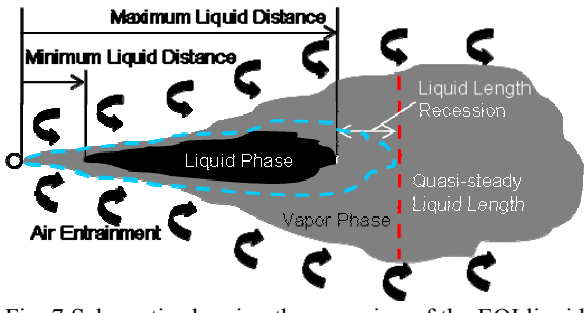

Fig. 7 Schematic showing the recession of the EOI liquid spray.

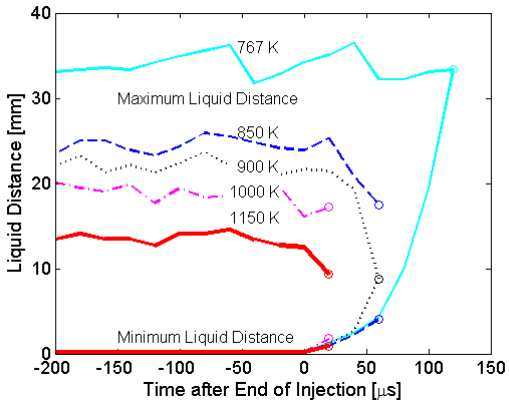

Fig. 9 Effect of ambient temperature on maximum and minimum liquid distances for conditions of Fig. 8.

The modeling results (Fig. 12) show that the predicted quasi-steady liquid lengths are similar to the experiments (Fig. 8) before EOI. Then, during injection-rate ramp-down, but prior to EOI (-10 μs), the liquid boundary begins to shrink for the 1150-K and 900-K conditions. This trend continues for the 1150-K and 900-K conditions up until 40 μs AEI. The liquid boundary for 767-K condition, however, does not recede from the quasi-steady liquid length (no liquid length recession). During this time, the liquid boundary tends to shrink towards the center of the jet for all temperatures, but it is particularly noticeable for the 767-K condition. The model shows that the liquid spray structure even separates at 767 K, leaving a section of liquid downstream near the quasi-steady liquid length at 50 μs AEI, similar to the experiments.

The modeling trends discussed above generally follow those observed in the experiment. For example, Figs. 8-9 showed that a liquid length recession exists at high ambient temperature, but none exists for the low-temperature, 767-K condition. The faster evaporation after EOI at high temperature also matches experimental trends. However, the model does appear to have a deficiency for prediction of liquid vaporization in the near-nozzle (less than 5 mm) region. Liquid remains

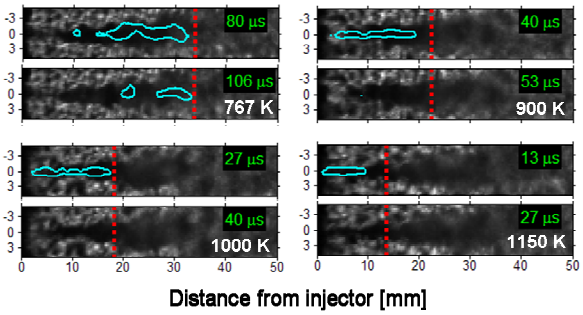

Fig. 10 Liquid-phase spray boundary overlaid on shadowgraph images for various ambient densities. Near-complete vaporization timings after end of injection (AEI) are shown. Dashed lines are quasi-steady spray tip penetrations. Ambient temperature is 900 K.

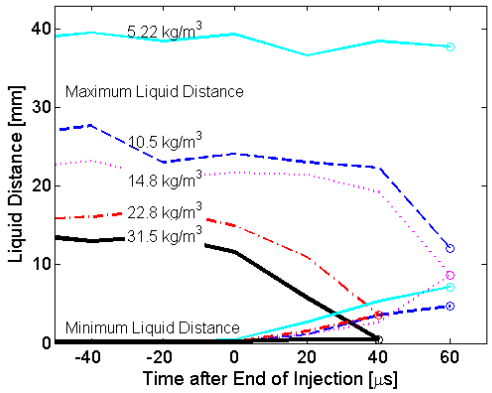

Fig. 11 Effect of ambient density on maximum and minimum liquid distances for conditions of Fig. 10.

near the injector in the model predictions while none was observed in the experiment. We believe that this deficiency is due to a failure to account for diffusion mixing near the injector after EOI, where the lateral length scales of the conical jet are very small. We therefore generally disregard predictions in this very near-injector region.

Model predictions for the ambient entrainment rate relative to the fuel mass flux provide further information about the cause for differences in liquid vaporization after EOI for variation in ambient temperature. Figure 13 shows the time sequence of the relative entrainment rate versus a distance from the injector. The rate given is a ratio of air mass flux entrainment per fuel mass flux for *EOI spray* to air mass flux entrainment per fuel mass flux for *quasi-steady spray* of Siebers model [5], which

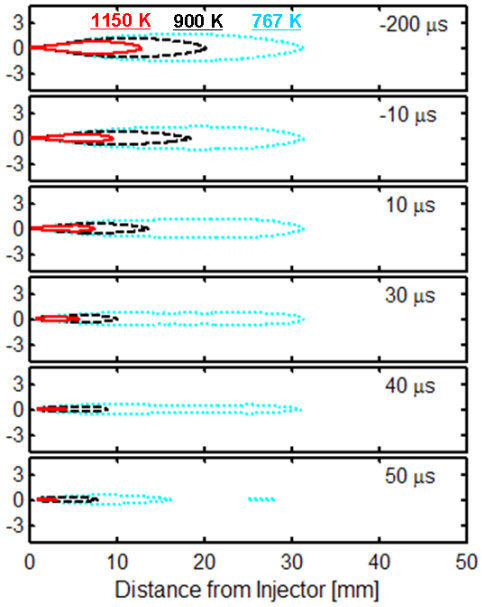

Fig. 12 Time sequence of liquid-phase spray from modeling for various ambient temperatures. Time after end of injection (AEI) is given at the upper-right corner. Ambient density 14.8 kg/m^3.

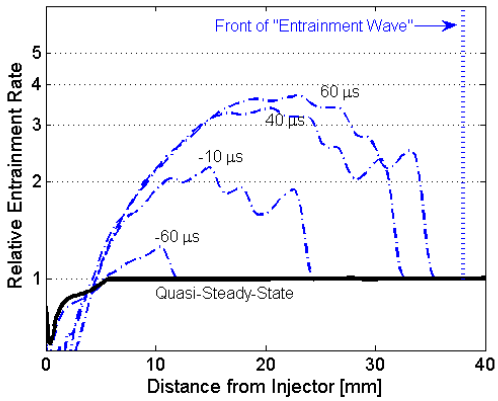

Fig. 13 Relative entrainment rate versus axial distance from injector for various times after end of injection. Ambient density is 14.8 kg/m^3.

can be expressed as:

$$\textit{Relative Entrainment Rate} = \frac{\left(\frac{\dot{m}_a(x)}{\dot{m}_f(x)}\right)_{EOI}}{\left(\frac{\dot{m}_a(x)}{\dot{m}_f(x)}\right)_{Siebers}} \quad (1)$$

Figure 13 shows that a slower fuel delivery increases the relative entrainment rate, thereby enhancing fuel-ambient mixing. The declining fuel mass flow rate (Fig. 6) and near-constant spreading angle measured after EOI (Fig. 5) contribute to this behavior. However, the increased relative entrainment does not affect all downstream regions of the jet equally. The increased entrainment begins as a small wave near 10 mm from the injector during the start of injection-rate ramp-down (-60 µs AEI). This "entrainment wave" then travels downstream while the fuel mass flow rate decreases to zero. At 40 µs AEI, the peak of the wave reaches near 20 mm, which is the quasi-steady length for the 900-K condition. Note that liquid spray began to recede experimentally at this timing (Fig. 5). Liquid-phase fuel vaporization is accelerated at distances closer to the injector because of this enhanced mixing region.

The entrainment wave tends to affect the liquid-phase tip vaporization early for high-temperature conditions because the quasi-steady liquid length is closer to the nozzle. The enhanced mixing can even occur when the injection rate decreases, but prior to EOI. As a result, the maximum liquid distance decreases either prior to EOI or shortly after EOI depending on the progress of the entrainment wave. For example, receding of the liquid spray was documented in both the experiment and the model jet at 1150 K and 900 K.

On the other hand, the liquid spray at low ambient temperature (767 K) requires a much longer time for the entrainment wave to reach the quasi-steady liquid length. At 40 µs AEI, the peak of the wave has traveled only one-half of the quasi-steady liquid length measured for the 767-K condition. This entrainment wave actually divides the liquid region into two sections, as was shown in Fig. 13, leaving the downstream section to vaporize near the quasi-steady liquid length. Also, model inaccuracies in the near-nozzle region (discussed above) do not accurately represent the complete vaporization that experimentally occurs near the nozzle for the 767-K condition. However, the model does show that the lack of liquid recession for this low-temperature condition is caused by an entrainment wave that has yet to reach the downstream, quasi-steady liquid length.

Jet model simulations were also performed for the ambient density variation from Figs. 10-11. Figure 14 shows the time sequence of liquid-phase boundaries while relative entrainment rate results are shown in Fig. 15 at 60 µs AEI. The general experimental results are again captured by the jet model. In particular, a liquid length recession is predicted at high ambient density, while a separation in the liquid border, leaving liquid near the quasi-steady length, is predicted at low ambient

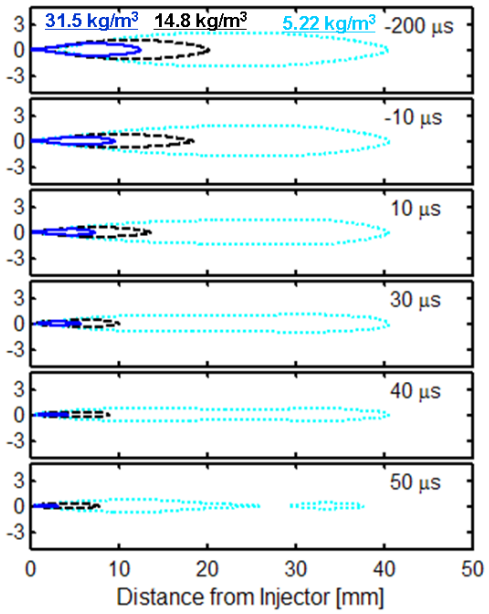

Fig. 14 Time sequence of liquid-phase spray boundary from modeling for various ambient densities. Time after end of injection (AEI) is given at the upper-right corner. Ambient temperature is 900 K.

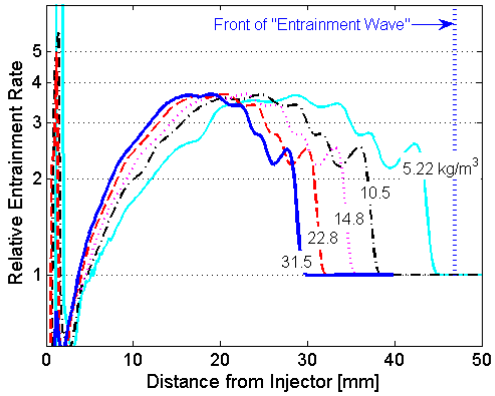

Fig. 15 Relative entrainment rate over a distance from injector for ambient densities at 60 µs AEI. Ambient temperature is 900 K.

density (5.2 kg/m^3).

Figure 15 shows that the entrainment wave travels downstream faster at lower ambient density, a result related to the faster jet penetration at low density. However, the entrainment wave tends to reach the quasi-steady liquid length more quickly at high ambient density rather than low ambient density. For example, at a density of 31.5 kg/m^3, the quasi-steady liquid length is about 10 mm and the peak of the entrainment wave travels 20 mm at 60 µs AEI. The enhanced mixing therefore causes a liquid length recession after EOI. By contrast, the peak of the entrainment wave lies upstream of the quasi-steady liquid length for 5.22 kg/m^3 at 60 µs AEI. Consequently, the liquid boundary separates and

liquid remains downstream near the quasi-steady liquid length.

The success of the discrete control-volume jet model in capturing the experimental liquid length recession with respect to ambient temperature and density is encouraging. Although it is a simplification of real jet profiles, the model appears to adequately represent the underlying physics of fuel-ambient mixing after EOI. The model shows that the position of the entrainment wave determines if liquid recedes from, or reaches, the quasi-steady liquid length after EOI.

CONCLUSIONS

An experimental study was performed to extend the understanding of liquid-phase fuel penetration and vaporization in sprays from quasi-steady-state to transient, end-of-injection (EOI) conditions. Experiments were conducted in an optically-accessible, constant-volume vessel at non-reacting conditions at high temperature and pressure. High-speed Mie-scatter and shadowgraph imaging provided time-resolved information about liquid-phase penetration, vapor distribution, and spreading angle after EOI.

Results show that the maximum liquid penetration distance typically decreases (recedes back toward the nozzle) from the quasi-steady-state liquid length after EOI. However, low-density and low-temperature conditions have no liquid length recession. Shadowgraph vapor-phase imaging shows that the jet spreading angle does not decrease after EOI. Together with a decreasing fuel mass delivery rate during injection-rate ramp-down, these results show that fuel-ambient mixing is enhanced in the near-nozzle region after EOI.

A one-dimensional transient jet entrainment model employing discrete control volumes and a polynomial jet cross-sectional velocity and mass clarifies details of the mixing after EOI. The model, coupled with the assumption of mixing-limited spray vaporization and constant jet spreading angle, showed that a mass and momentum transport after EOI generates a wave of increased entrainment that travels downstream until it reaches the liquid-phase tip of the spray. Depending upon the position of the entrainment wave relative to the quasi-steady liquid length, the enhanced mixing could either cause the liquid length to recede back toward the injector, or create a break in the liquid spray, with the liquid tip remaining near the quasi-steady liquid length. The above trends were observed experimentally and successfully represented by the jet model over a range of ambient temperature and ambient density.

Acknowledgements

Support for this research was provided by the U.S. Department of Energy, Office of Vehicle Technologies. The research was performed at the Combustion Research Facility, Sandia National Laboratories, Livermore, California. Sandia is a multiprogram laboratory operated by Sandia Corporation, a Lockheed Martin Company, for the United States Department of Energy's National Nuclear Security Administration under contract DE-AC04-94AL85000. The authors thank Kyle Kattke for the contribution on the model development.

NOMENCLATURE

AEI: After End of Injection
ASI: After Start of Injection
CMOS: Complementary Metal Oxide Semiconductor
EOI: End Of Injection
F/A: Fuel to Air ratio
FWHM: Full Width at Half Maximum
HeNe: Helium-Neon
SOI: Start Of Injection
Nd:YAG: Neodymium-doped Yttrium Aluminum Garnet
UHC: Unburned Hydrocarbon

REFERENCES

[1] Smallwood, G. and Gulder, O., Atomization and Sprays, 10:355–386 (2000).
[2] Li, S.-W., Kosaka, H., and Kamimoto, T., SAE Trans 103:1017-1025, No. 941924 (1994).
[3] Ishikawa, N. and Zhang, L. SAE Tech. Pap. Ser. 1999-01-0522 (1999).
[4] Browne, K., Partridge, I., and Greeves, G., SAE Tech. Pap. Ser. 860223 (1986).
[5] Dent, J.C., SAE Trans 80:1881-1884, No. 710571 (1971).
[6] Hiroyasu, H. and Arai, M., SAE Trans 99:1050-1061, No. 900475 (1990).
[7] Kamimoto, T., Yokota, H., and Kobayashi, H., SAE Trans 96:783-791, No. 871610 (1987).
[8] Kim, T. and Ghandhi, J. B., Atomization and Sprays, 13:535-559 (2003).
[9] Desantes, J.M., López, J.J., Garcia, J.M., and Pastor, J.M., Atomization and Sprays, 17:193-231 (2007).
[10] Naber J. and Siebers, D.L., SAE Trans 105:82-111, No. 960034 (1996).
[11] Siebers, D.L., SAE Tech. Pap. Ser. 1999-01-0528 (1999).
[12] Akagawa, H., Miyamoto, T., Harada, A., Sasaki, S., Shimazaki, N., Hashizume, T., and Tsujimura, K., SAE Trans, 108:120-132 No. 1999-01-0183 (1999).
[13] Kanda, T., Hakozaki, T., Uchimoto, T., Hatano, J., Kitayama, N., and Sono, H., SAE Tech. Pap. Ser. 2005-01-0378 (2005).
[14] Kook, S., Park, S., and Bae, C., Energy Fuels, 22:331-337 (2008).
[15] Bruneaux, G., SAE Trans 114:1444-1461, No. 2005-01-2100 (2005).
[16] Musculus, M.P.B., Lachaux, T., Pickett, L.M., and Idicheria, C.A., SAE Tech. Pap. Ser. 2007-01-0907 (2007).
[17] Engine Combustion Network Experimental Data archive, http://www.ca.sandia.gov/ecn
[18] Abramovich, G.N., The Theory of Turbulent Jets, The M.I.T. Press, Cambridge, Massachusetts, 1963, pp. 180-181.
[19] Pickett, L.M. and Hoogterp, L., SAE Tech. Pap. Ser. 2008-01-1083 (2008).